Modeling, Analysis and Testing of Autonomous Operation of an Inverter-Based Microgrid

Nagaraju Pogaku, Milan Prodanović, *Member, IEEE*, Tim C Green, *Senior Member, IEEE*

***Abstract*— This paper deals with the modeling and analyzing the autonomous operation of inverter-based microgrids. Each sub-module is modeled in state-space form and are combined together on a common reference frame. The complete model is linearized around an operation point and its system matrix is obtained to derive the eigenvalues. Eigenvalues (termed '*modes*') provide the information on the frequency and damping of oscillatory components in the transient response. A sensitivity analysis is also presented which helps in identifying the origin of each of the modes and possible feedback signal to design the appropriate controller to improve the system stability. Experimental results of a prototype microgrid are provided to verify the results obtained from the model.**

***Index Terms*— microgrid, small-signal stability, inverter, parallel operation.**

I. INTRODUCTION

Recent innovations in small-scale distributed power generation systems combined with technological advancements in power electronic systems led to the concepts of future network technologies such as microgrids. These small power systems are gaining popularity because they offer increased reliability and efficiency, uses environmental friendly renewable energy and other forms of distributed generation [1]. Many forms of distributed generation (DG) systems such as fuel-cells, photo-voltaic and micro-turbines are interfaced to the network through power electronic converters [2] [3] [4]. These interfacing devices make them more flexible in their operation and control compared to the conventional power systems. However, due to their negligible physical inertia they also make the system potentially prone to network disturbances.

A microgrid can be operated either in grid connected mode or in stand-alone mode. In grid connected mode, most of the system-level dynamics are dictated by the main grid due to the relatively small size of micro sources. In stand-alone mode, the system dynamics are dictated by micro sources, the network and the nature of the power regulation control.

One of the important aspects of such a low inertia systems is their small-signal stability. Previous dynamic analysis of stand-alone systems is carried out by assuming an ideal inverter as in[5]. This means that the closed-loop inner controllers (voltage and current) are assumed to be able to generate the required output at the inverter terminals and they do not have any effect on the small signal stability. This assumption is based on the fact that the closed-loop bandwidth of the inverter is well above the bandwidth of power sharing controllers. The modeling approach presented in [6] concentrates on individual inverter stability issues when connected to a stiff ac bus. However, a complete analysis of inverter-based microgrids involving fast acting controllers is necessary.

In this paper a systematic approach to model an inverter-based microgrid is presented. Each DG inverter will have an outer power loop based on droop control to share the fundamental real and reactive powers with other DGs. Inverter internal controls include voltage and current controllers which are designed to reject high frequency disturbances and damp the output LC filter to avoid any resonance with external network. A small-signal state-space model is constructed including the controls, output filter and coupling inductor on a synchronous reference frame whose rotation frequency is set by the power controller of individual inverter. An arbitrary choice is made to select one inverter frame as the common reference frame and all the network state equations are represented on this common reference frame. All other inverters are translated to this common reference frame using simple transformation techniques as used with synchronous machine systems.

Once the small-signal model has been formed, eigenvalues (or *modes*) are identified that express the typical frequency components present and their available damping. In such a way, the relation between system stability and system parameters, including the gains of controllers, is established. A sensitivity analysis is then conducted which provides the sensitivity of different modes to the system state variables and point out the role of each controller in forming of these modes.

II. MICROGRID MODEL IN AUTONOMOUS OPERATION

A typical characteristic of a microgrid is that it can be operated either in grid connected or in islanded (autonomous) mode. Normally, when a microgrid is operated in grid connected mode the micro sources act as constant power sources which means that they are controlled to inject the demanded power in to the network. In autonomous mode the micro sources are controlled to supply all the power needed by the local loads while maintaining the voltage and frequency within the allowed limits. Autonomous operation of a microgrid might be initiated for either of the following two reasons. First, because of pre-planned (intentional) islanding due to maintenance or economical reasons. Depending on the market situation the owner of a microgrid can chose between autonomous and grid connected modes [7]. Second, because of un-planned (un-intentional) islanding due to the failure of the main grid caused by a network fault.

Autonomous operation is realised by opening the isolating switch (shown in Fig. 1) which disconnects the microgrid

The authors are with the Department of Electrical and Electronics Engineering, Imperial College London, London SW7 2BT, UK (nagaraju.pogaku@imperial.ac.uk)

from the main grid. Once the microgrid is isolated the micro sources feeding the system are responsible for maintaining the voltage and frequency while sharing the power. During the autonomous operation it is important to avoid the overloading of inverters so it is also important to ensure that changes in load are taken by inverters in a pre-determined manner. Control techniques based on a communication link, such as the master-slave approach [8], can be adapted in systems where micro sources are connected to a common bus or located in close proximity. However, communication link makes the system more expensive and less reliable. Also, in a typical microgrid micro sources can be located far away from each other making communication link less attractive. Control techniques based on local measurements which do not require expensive communication facilities have been proposed [9]. In this paper the later method is adopted.

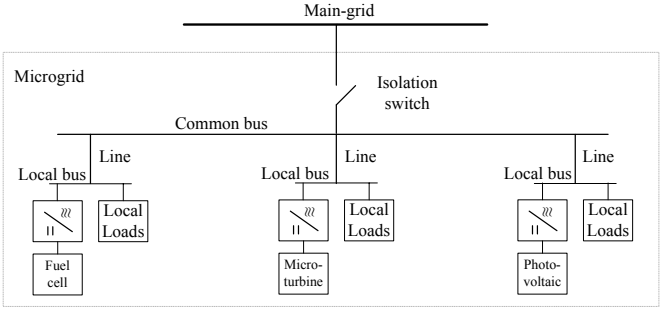

Fig. 1. A typical structure of inverter-based microgrid

The modeling approach presented in this paper divides the whole system into three major sub-modules; inverter, network and loads (Fig.2). Each inverter is modeled on its individual reference frame whose rotation frequency is set by its local power sharing controller. The inverter model includes the power sharing controller dynamics, output filter dynamics, coupling inductor dynamics and voltage and current controller dynamics. This last element introduces high frequency dynamics which are apparent at peak and light load conditions and during large changes in load. The small-signal flow among the sub-modules shown in Fig. 2 will be explained in the following sections.

Network dynamics are generally neglected in small-signal modeling of conventional power systems. The reason behind this is that the time constants of rotating machines and their controls are much larger than those of the network. In the case of microgrids, the micro sources are connected through inverters whose response times are very small and network dynamics would influence the system stability. Previous work [5] on small-signal modeling of parallel connected inverters was carried out without considering the network dynamics.

Here, the state equations of the network and the loads are represented on the reference frame of one of the individual inverters. This reference frame is considered as the common reference frame. All the other inverters are translated to this common reference frame using the transformation technique [10] depicted in Fig. 3 and defined in (1). Here, the axis set $(D-Q)$ is the common reference frame rotating

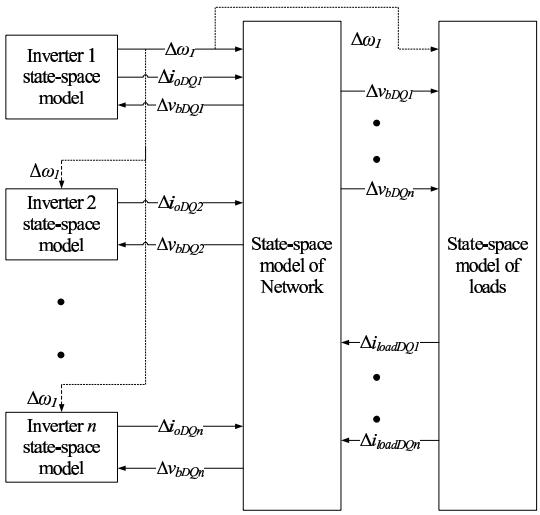

Fig. 2. Block diagram of complete small-signal state-space model of a microgrid

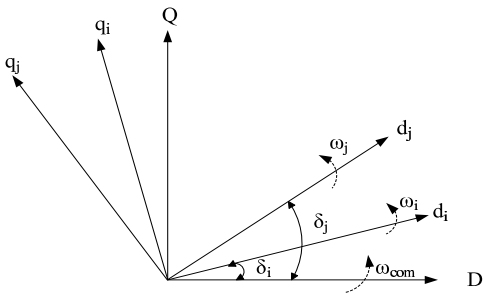

Fig. 3. Reference frame transformation

at a frequency ω_{com}, where as axes $(d-q)_i$ and $(d-q)_j$ are the reference frame of i^{th} and j^{th} inverters rotating at ω_i and ω_j, respectively .

$$\left[\ f_{DQ}\ \right] = \left[\ T_i\ \right]\left[\ f_{dq}\ \right] \tag{1}$$

$$\left[\ T_i\ \right] = \begin{bmatrix} cos(\delta_i) & -sin(\delta_i) \\ sin(\delta_i) & cos(\delta_i) \end{bmatrix} \tag{2}$$

In (1) and (2), δ_i is the angle of the reference frame of i^{th} inverter with respect to the common reference frame. In the following sections the internal modeling of all the three modules is discussed more in detail.

A. State-Space Model of Voltage Source Inverter

Voltage source inverter is commonly used to interface distributed generators to the network. Fig. 4 shows the block diagram of an inverter connected to the microgrid. The power processing section consists of a three-leg inverter, an output LC filter and coupling inductor. Assuming an ideal source from the DG side, the dc bus dynamics can be neglected. With the realization of high switching frequencies (4-10 kHz), the switching process of the inverter may also be neglected.

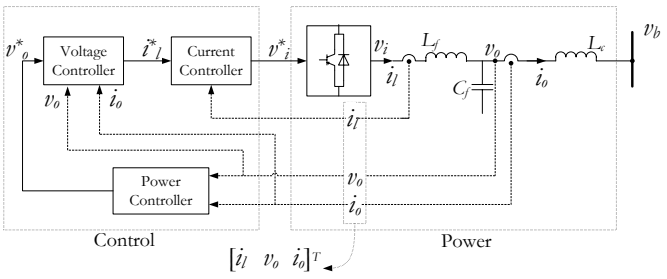

Fig. 4. DG Inverter Block Diagram

The control section can be divided into three different parts. First is an external power control loop which sets the magnitude and frequency (and hence phase) for the fundamental component of the inverter output voltage according to its droop characteristics set for the real and reactive powers. Harmonic power sharing has been treated as an additional function with a different control topology [11]. The second and third parts of the control system are the voltage and current controllers, which are designed to reject high frequency disturbances and provide sufficient damping for the output LC filter [12] [13].

In this section a state space model is presented for all of the subsystems: control loops, output filter and coupling inductor. The model is constructed in a rotational reference frame set by the external power controller of individual inverter.

1) Power Controller: The basic idea behind the droop control is to mimic the governor of a synchronous generator. In a conventional power system, synchronous generators will share any increase in the load by decreasing the frequency according to their governor droop characteristic. This principle is implemented in inverters by decreasing the reference frequency when there is an increase in the load. Similarly, reactive power is shared by introducing a droop characteristic in voltage magnitude.

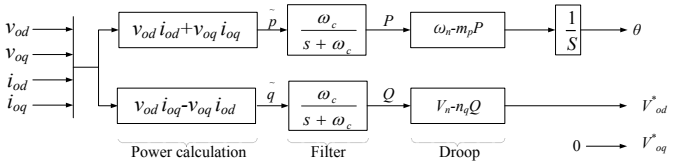

Fig. 5. Power Controller

As shown in Fig.5, instantaneous active and reactive power components $\tilde{p}$ and $\tilde{q}$ are calculated from the measured output voltage and output current as in (3).

$$\begin{aligned} \tilde{p} &= v_{od} i_{od} + v_{oq} i_{oq} \\ \tilde{q} &= v_{od} i_{oq} - v_{oq} i_{od} \end{aligned} \tag{3}$$

The instantaneous power components are passed through low-pass filters, shown in (4), to obtain the real and reactive powers P and Q corresponding to the fundamental component. ω_c represents the cut-off frequency of low-pass filters.

$$P = \frac{s}{s+\omega_c}\tilde{p}, \quad Q = \frac{s}{s+\omega_c}\tilde{q} \tag{4}$$

The real power sharing between inverters is obtained by introducing an artificial droop in the inverter frequency as in (5). The frequency ω is dropped according to the droop gain (m_p) and phase is set by integrating the frequency. In the following equations ω_n will represent the nominal frequency set-point.

$$\omega = \omega_n - m_p P, \quad \dot{\theta} = \omega \tag{5}$$

Similarly, to share the reactive power among multiple inverters, a droop is introduced in voltage magnitude as given in (6). Here, V_n stands for the nominal set point of d-axis output voltage. The control strategy is chosen such that the output voltage magnitude reference is aligned to the d-axis of the inverter reference frame, where as q-axis reference is set to zero.

$$v_{od}^* = V_n - n_q\, Q, \quad v_{oq}^* = 0 \tag{6}$$

The droop gains m_p and n_q are calculated using equation (7) for the given range of frequency and voltage magnitude.

$$m_p = \frac{\omega_{max} - \omega_{min}}{P_{max}}, \quad n_q = \frac{V_{od\ max} - V_{od\ min}}{Q_{max}} \tag{7}$$

In small-signal analysis the inverter angle θ can be written as in (8), where δ is the angle of the inverter reference frame seen from an arbitrary common reference frame, similar to power angle of a synchronous generator. It is to be understood that each individual inverter is modeled on the reference frame determined by its own power controller.

$$\theta = \omega_n t + \delta \tag{8}$$

Hence, from equations (5) and (8),

$$\dot{\delta} = -m_p\, P \tag{9}$$

By linearizing and rearranging above equations, the small-signal power controller model can be written in a state-space form as in (10). The outputs of the power controller are the output voltage reference Δv_o^* and small-signal variation of frequency $\Delta\omega$. The matrices are defined in (11).

$$\begin{bmatrix} \dot{\Delta\delta} \\ \Delta P \\ \Delta Q \end{bmatrix} = A_P \begin{bmatrix} \Delta\delta \\ \Delta P \\ \Delta Q \end{bmatrix} + B_P \begin{bmatrix} \Delta i_l \\ \Delta v_o \\ \Delta i_o \end{bmatrix}$$
$$\begin{bmatrix} \Delta\omega \\ \Delta v_o^* \end{bmatrix} = \begin{bmatrix} C_{P\omega} \\ C_{Pv} \end{bmatrix} \begin{bmatrix} \Delta\delta \\ \Delta P \\ \Delta Q \end{bmatrix} \tag{10}$$

$$A_P = \begin{bmatrix} 0 & -m_p & 0 \\ 0 & -\omega_c & 0 \\ 0 & 0 & -\omega_c \end{bmatrix} \quad C_{P\omega} = \begin{bmatrix} 0 & -m_p & 0 \end{bmatrix}$$
$$C_{Pv} = \begin{bmatrix} 0 & 0 & -n_q \\ 0 & 0 & 0 \end{bmatrix}$$
$$B_P = \begin{bmatrix} 0 & 0 & 0 & 0 & 0 & 0 \\ 0 & 0 & \omega_c I_{od} & \omega_c I_{oq} & \omega_c V_{od} & \omega_c V_{oq} \\ 0 & 0 & \omega_c I_{oq} & -\omega_c I_{od} & -\omega_c V_{oq} & \omega_c V_{od} \end{bmatrix} \tag{11}$$

The d and q axis components of voltages and currents are joined to form vectors as in (12) to allow a simpler system presentation.

$$\Delta v_o^* = \begin{bmatrix} v_{od}^* & v_{oq}^* \end{bmatrix}^T, \Delta i_l = \begin{bmatrix} i_{ld} & i_{lq} \end{bmatrix}^T$$
$$\Delta v_o = \begin{bmatrix} v_{od} & v_{oq} \end{bmatrix}^T, \Delta i_o = \begin{bmatrix} i_{od} & i_{oq} \end{bmatrix}^T \quad (12)$$

2) Voltage Controller: Fig. 6 shows the voltage controller block diagram including all feed-back and feed-forward terms. Output voltage control is achieved with a standard PI controller. Corresponding state equations are

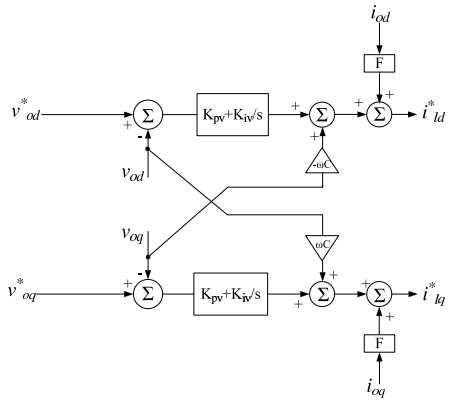

Fig. 6. Voltage Controller

$$\frac{d\phi_d}{dt} = v_{od}^* - v_{od}, \quad \frac{d\phi_q}{dt} = v_{oq}^* - v_{oq} \quad (13)$$

along with the algebraic equations

$$i_{ld}^* = F\ i_{od} - \omega_n\ C_f\ v_{oq} + K_{pv}\ (v_{od}^* - v_{od}) + K_{iv}\ \phi_d \quad (14)$$

$$i_{lq}^* = F\ i_{oq} + \omega_n\ C_f\ v_{od} + K_{pv}\ (v_{oq}^* - v_{oq}) + K_{iv}\ \phi_q \quad (15)$$

Equation (16) represents the linearized small-signal state-space form of voltage controller. Here, the input to the subsystem is split in to two terms: the reference input and feedback inputs.

$$\begin{bmatrix} \dot{\Delta\phi} \end{bmatrix} = \begin{bmatrix} 0 \end{bmatrix} \begin{bmatrix} \Delta\phi \end{bmatrix} + B_{V1} \begin{bmatrix} \Delta v_o^* \end{bmatrix} + B_{V2} \begin{bmatrix} \Delta i_l \\ \Delta v_o \\ \Delta i_o \end{bmatrix} \quad (16)$$

In equation (16),

$$\Delta\phi = \begin{bmatrix} \Delta\phi_d & \Delta\phi_q \end{bmatrix}^T \quad (17)$$

$$B_{V1} = \begin{bmatrix} 1 & 0 \\ 0 & 1 \end{bmatrix}, \quad B_{V2} = \begin{bmatrix} 0 & 0 & -1 & 0 & 0 & 0 \\ 0 & 0 & 0 & -1 & 0 & 0 \end{bmatrix} \quad (18)$$

$$\begin{bmatrix} \Delta i_l^* \end{bmatrix} = C_V \begin{bmatrix} \Delta\phi \end{bmatrix} + D_{V1} \begin{bmatrix} \Delta v_o^* \end{bmatrix} + D_{V2} \begin{bmatrix} \Delta i_l \\ \Delta v_o \\ \Delta i_o \end{bmatrix} \quad (19)$$

$$C_V = \begin{bmatrix} K_{iv} & 0 \\ 0 & K_{iv} \end{bmatrix}, \quad D_{V1} = \begin{bmatrix} K_{pv} & 0 \\ 0 & K_{pv} \end{bmatrix}$$
$$D_{V2} = \begin{bmatrix} 0 & 0 & -K_{pv} & -\omega_n C_f & F & 0 \\ 0 & 0 & \omega_n C_f & -K_{pv} & 0 & F \end{bmatrix} \quad (20)$$

3) Current Controller: Fig. 7 shows the current controller structure. Output filter inductor current control is achieved with a standard PI controller. Corresponding state equations are

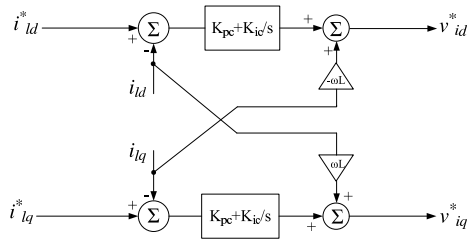

Fig. 7. Current Controller

$$\frac{d\gamma_d}{dt} = i_{ld}^* - i_{ld} \quad \frac{d\gamma_q}{dt} = i_{lq}^* - i_{lq} \quad (21)$$

along with the algebraic equations

$$v_{id}^* = v_{od} - \omega_n\ L_f\ i_{lq} + K_{pc}\ (i_{ld}^* - i_{ld}) + K_{ic}\ \gamma_d \quad (22)$$

$$v_{iq}^* = v_{oq} + \omega_n\ L_f\ i_{ld} + K_{pc}\ (i_{lq}^* - i_{lq}) + K_{ic}\ \gamma_q \quad (23)$$

Equation (24) represents the linearized small-signal state-space form of current controller,

$$\begin{bmatrix} \dot{\Delta\gamma} \end{bmatrix} = \begin{bmatrix} 0 \end{bmatrix} \begin{bmatrix} \Delta\gamma \end{bmatrix} + B_{C1} \begin{bmatrix} \Delta i_l^* \end{bmatrix} + B_{C2} \begin{bmatrix} \Delta i_l \\ \Delta v_o \\ \Delta i_o \end{bmatrix} \quad (24)$$

where,

$$\Delta\gamma = \begin{bmatrix} \Delta\gamma_d & \Delta\gamma_q \end{bmatrix}^T \quad (25)$$

$$B_{C1} = \begin{bmatrix} 1 & 0 \\ 0 & 1 \end{bmatrix}, \quad B_{C2} = \begin{bmatrix} -1 & 0 & 0 & 0 & 0 & 0 \\ 0 & -1 & 0 & 0 & 0 & 0 \end{bmatrix} \quad (26)$$

$$\begin{bmatrix} \Delta v_i^* \end{bmatrix} = C_C \begin{bmatrix} \Delta\gamma \end{bmatrix} + D_{C1} \begin{bmatrix} \Delta i_l^* \end{bmatrix} + D_{C2} \begin{bmatrix} \Delta i_l \\ \Delta v_o \\ \Delta i_o \end{bmatrix} \quad (27)$$

$$C_C = \begin{bmatrix} K_{ic} & 0 \\ 0 & K_{ic} \end{bmatrix}, \quad D_{C1} = \begin{bmatrix} K_{pc} & 0 \\ 0 & K_{pc} \end{bmatrix}$$
$$D_{C2} = \begin{bmatrix} -K_{pc} & -\omega_n L_f & 0 & 0 & 0 & 0 \\ \omega_n L_f & -K_{pc} & 0 & 0 & 0 & 0 \end{bmatrix} \quad (28)$$

4) Output LC Filter and Coupling Inductance: Output LC filter and the coupling inductance small-signal model can be represented with the following state equations by assuming that inverter produces the demanded voltage ($v_i = v_i^*$).

$$\frac{di_{ld}}{dt} = \frac{-r_f}{L_f} i_{ld} + \omega\ i_{lq} + \frac{1}{L_f} v_{id} - \frac{1}{L_f} v_{od} \tag{29}$$

$$\frac{di_{lq}}{dt} = \frac{-r_f}{L_f} i_{lq} - \omega\ i_{ld} + \frac{1}{L_f} v_{iq} - \frac{1}{L_f} v_{oq} \tag{30}$$

$$\frac{dv_{od}}{dt} = \omega\ v_{oq} + \frac{1}{C_f} i_{ld} - \frac{1}{C_f} i_{od} \tag{31}$$

$$\frac{dv_{oq}}{dt} = -\omega\ v_{od} + \frac{1}{C_f} i_{lq} - \frac{1}{C_f} i_{oq} \tag{32}$$

$$\frac{di_{od}}{dt} = \frac{-r_c}{L_c} i_{od} + \omega\ i_{oq} + \frac{1}{L_c} v_{od} - \frac{1}{L_c} v_{bd} \tag{33}$$

$$\frac{di_{oq}}{dt} = \frac{-r_c}{L_c} i_{oq} - \omega\ i_{od} + \frac{1}{L_c} v_{oq} - \frac{1}{L_c} v_{bq} \tag{34}$$

Following equations represents the linearized small-signal state-space form of the LC filter and coupling inductance. Frequency ω_0 is the system steady-state frequency at the given operating point.

$$\begin{bmatrix} \dot{\Delta i_l} \\ \Delta v_o \\ \Delta i_o \end{bmatrix} = A_{LCL} \begin{bmatrix} \Delta i_l \\ \Delta v_o \\ \Delta i_o \end{bmatrix} + B_{LCL1} [\Delta v_i] + B_{LCL2} [\Delta v_{bdq}] + B_{LCL3} [\Delta \omega] \tag{35}$$

$$A_{LCL} = \begin{bmatrix} \frac{-r_{L_f}}{L_f} & \omega_0 & \frac{-1}{L_f} & 0 & 0 & 0 \\ -\omega_0 & \frac{-r_{L_f}}{L_f} & 0 & \frac{-1}{L_f} & 0 & 0 \\ \frac{1}{C_f} & 0 & 0 & \omega_0 & -\frac{1}{C_f} & 0 \\ 0 & \frac{1}{C_f} & -\omega_0 & 0 & 0 & -\frac{1}{C_f} \\ 0 & 0 & \frac{1}{L_c} & 0 & \frac{-r_{L_c}}{L_c} & \omega_0 \\ 0 & 0 & 0 & \frac{1}{L_c} & -\omega_0 & \frac{-r_{L_c}}{L_c} \end{bmatrix}$$

$$B_{LCL1} = \begin{bmatrix} \frac{1}{L_f} & 0 \\ 0 & \frac{1}{L_f} \\ 0 & 0 \\ 0 & 0 \\ 0 & 0 \\ 0 & 0 \end{bmatrix} \quad B_{LCL2} = \begin{bmatrix} 0 & 0 \\ 0 & 0 \\ 0 & 0 \\ 0 & 0 \\ -\frac{1}{L_c} & 0 \\ 0 & -\frac{1}{L_c} \end{bmatrix}$$

$$B_{LCL3} = \begin{bmatrix} I_{lq} & -I_{ld} & V_{oq} & -V_{od} & I_{oq} & -I_{od} \end{bmatrix}^T \tag{36}$$

5) Complete inverter model: To connect an inverter to the whole system the output variables need to be converted on to common reference frame. In this case the output variables of an inverter are the output currents represented as vector Δi_{oDQ}. Using the transformation technique introduced in (1) and (2), the small-signal output current on common reference frame can be obtained, as in (37). The small signal equivalent of the reference transformation is shown in Fig. 8.

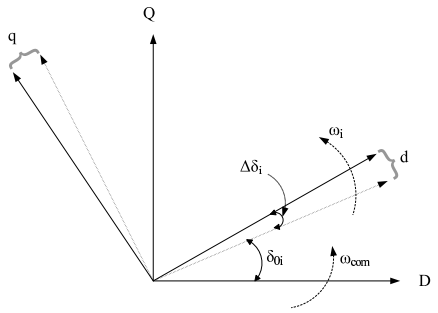

Fig. 8. Small-signal equivalent of reference frame transformation

$$\begin{bmatrix} \Delta i_{oDQ} \end{bmatrix} = [T_S] \begin{bmatrix} \Delta i_o \end{bmatrix} + [T_C] \begin{bmatrix} \Delta \delta \end{bmatrix} \tag{37}$$

where,

$$T_S = \begin{bmatrix} cos(\delta_0) & -sin(\delta_0) \\ sin(\delta_0) & cos(\delta_0) \end{bmatrix}$$

$$T_C = \begin{bmatrix} -I_{od} sin(\delta_0) - I_{oq} cos(\delta_0) \\ I_{od} cos(\delta_0) - I_{oq} sin(\delta_0) \end{bmatrix} \tag{38}$$

$$\Delta\delta = \int (\Delta\omega - \Delta\omega_{com}) \tag{39}$$

Similarly, the input signal to the inverter model is the bus voltage which is expressed on common reference frame. The bus voltage can be converted on to individual inverter reference frame using reverse transformation, given by (40),

$$\begin{bmatrix} \Delta v_{bdq} \end{bmatrix} = \left[T_S^{-1}\right] \begin{bmatrix} \Delta v_{bDQ} \end{bmatrix} + \left[T_V^{-1}\right] \begin{bmatrix} \Delta \delta \end{bmatrix} \tag{40}$$

where,

$$T_V^{-1} = \begin{bmatrix} -V_{bD} sin(\delta_0) + V_{bQ} cos(\delta_0) \\ -V_{bD} cos(\delta_0) - V_{bQ} sin(\delta_0) \end{bmatrix} \tag{41}$$

It is to be noted that the inverter whose reference frame is taken as the common reference frame has to provide its reference frequency $\Delta\omega_{com}$ to all the sub-modules as shown in (39). Also, care should be taken to introduce this modification in the power controller output (10).

A complete state-space small-signal model of inverter can be obtained using the state models of power controller, voltage controller , current controller and output LCL filter, given by equations (10), (16), (19), (24), (27), (35), (37) and (40),

$$[\dot{\Delta x_{invi}}] = A_{INVi} [\Delta x_{invi}] + B_{INVi} [\Delta v_{bDQi}] \tag{42}$$

$$\begin{bmatrix} \Delta\omega_i \\ \Delta i_{oDQi} \end{bmatrix} = \begin{bmatrix} C_{INV\omega i} \\ C_{INVci} \end{bmatrix} [\Delta x_{invi}] \tag{43}$$

where,

$$\Delta x_{invi} = [\Delta\delta_i\ \Delta P_i\ \Delta Q_i\ \Delta\phi_i\ \Delta\gamma_i\ \Delta i_{li}\ \Delta v_{oi}\ \Delta i_{oi}]^T \tag{44}$$

$$B_{INVi} = \begin{bmatrix} 0 \\ 0 \\ 0 \\ B_{LCL2} T_S^{-1} \end{bmatrix} \tag{46}$$

$$A_{INVi} = \begin{bmatrix} A_{Pi} & 0 & 0 & B_{Pi} \\ B_{V1i}C_{Pvi} & 0 & 0 & B_{V2i} \\ B_{C1i}D_{V1i}C_{Pvi} & B_{C1i}C_{Vi} & 0 & B_{C1i}D_{V2i} + B_{C2i} \\ \begin{matrix} B_{LCL1i}D_{C1i}D_{V1i}C_{Pvi}+ \\ B_{LCL2i}\left[T_{Vi}^{-1}\ 0\ 0\right] + \\ B_{LCL3i}C_{P\omega i} \end{matrix} & B_{LCL1i}D_{C1i}C_{Vi} & B_{LCL1i}C_{Ci} & \begin{matrix} A_{LCLi}+ \\ B_{LCL1i}\left(D_{C1i}D_{V2i} + D_{C2i}\right) \end{matrix} \end{bmatrix} \begin{matrix} \Delta\delta_i \\ \Delta P_i \\ \Delta Q_i \\ \Delta\phi_i \\ \Delta\gamma_i \\ \Delta i_{li} \\ \Delta v_{oi} \\ \Delta i_{oi} \end{matrix} \quad (45)$$

$$\text{states}$$

$$C_{INV\omega i} = \begin{cases} \left[\begin{array}{cccc} C_{PC\omega} & 0 & 0 & 0 \end{array}\right] & i = 1 \\ \left[\begin{array}{cccc} 0 & 0 & 0 & 0 \end{array}\right] & i \neq 1 \end{cases} \quad (47)$$

$$C_{INVci} = \left[\begin{array}{ccccc} \left[T_C\ 0\ 0\right] & 0 & 0 & \left[0\ 0\ T_S\right] \end{array}\right] \quad (48)$$

Now the states of all inverters in the system can be combined to form inverter state-space model and represented as in (49).

$$[\Delta x_{inv}] = [\Delta x_{inv1}\ \Delta x_{inv2}\ ...\ \Delta x_{inv\ s}]^T \quad (49)$$

B. Network Model

An example network of *n* lines and *m* nodes with *s* inverters and *p* load points is shown in Fig. 9. On a common reference frame the state equations of line current of i^{th} line connected between nodes *j* and *k* are

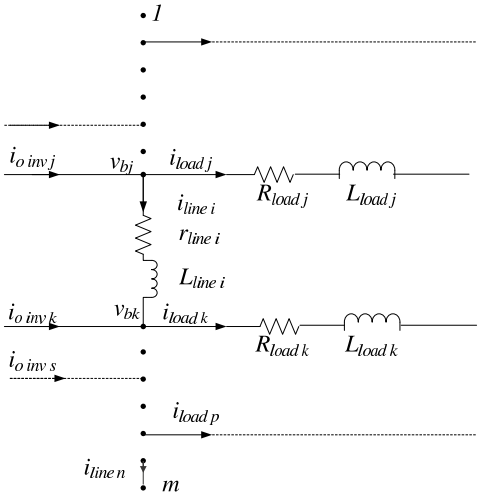

Fig. 9. Network representation

$$\frac{di_{lineDi}}{dt} = \frac{-r_{linei}}{L_{linei}} i_{lineDi} + \omega i_{lineQi} + \frac{1}{L_{linei}} v_{bDj} - \frac{1}{L_{linei}} v_{bDk} \quad (50)$$

$$\frac{di_{lineQi}}{dt} = \frac{-r_{linei}}{L_{linei}} i_{lineQi} - \omega i_{lineDi} + \frac{1}{L_{linei}} v_{bQj} - \frac{1}{L_{linei}} v_{bQk} \quad (51)$$

Hence, the small-signal state-space model of a network with *n* lines is given by (52).

$$\left[\begin{array}{c} \Delta\dot{i}_{line} \end{array}\right] = A_{NET}\left[\begin{array}{c} \Delta i_{line} \end{array}\right] + B_{1NET}\left[\Delta v_{bDQ}\right] + B_{2NET}\Delta\omega \quad (52)$$

In (52),

$$\left[\begin{array}{c} \Delta i_{line} \end{array}\right] = [\Delta i_{line\ 1}\ \Delta i_{line\ 2}\ ...\ \Delta i_{line\ n}]^T \quad (53)$$

$$\left[\begin{array}{c} \Delta v_{bDQ} \end{array}\right] = [\Delta v_{bDQ\ 1}\ \Delta v_{bDQ\ 2}\ ...\ \Delta v_{bDQ\ m}]^T \quad (54)$$

$$\Delta\omega = \Delta\omega_{com} \quad (55)$$

$$A_{NET} = \begin{bmatrix} A_{NET\ 1} & 0 & ... & 0 \\ 0 & A_{NET\ 2} & ... & 0 \\ ... & ... & ... & ... \\ 0 & 0 & ... & A_{NET\ n} \end{bmatrix}_{2n\times 2n} \quad (56)$$

$$B_{1NET} = \left[\begin{array}{c} B_{1NET\ 1}\ B_{1NET\ 2}\ ...\ B_{1NET\ n} \end{array}\right]^T$$
$$B_{2NET} = \left[\begin{array}{c} B_{2NET\ 1}\ B_{2NET\ 2}\ ...\ B_{2NET\ n} \end{array}\right]^T \quad (57)$$

where,

$$A_{NETi} = \begin{bmatrix} \frac{-r_{linei}}{L_{linei}} & \omega_0 \\ -\omega_0 & \frac{-r_{linei}}{L_{linei}} \end{bmatrix} B_{2NETi} = \begin{bmatrix} I_{lineQi} \\ -I_{lineDi} \end{bmatrix}$$
$$B_{1NETi} = \begin{bmatrix} ... & \frac{1}{L_{linei}} & 0 & ... & \frac{-1}{L_{linei}} & 0 & ... \\ ... & 0 & \frac{1}{L_{linei}} & ... & 0 & \frac{-1}{L_{linei}} & ... \end{bmatrix}_{2\times(2m)} \quad (58)$$

C. Load model

Although, many types of load can exist in microgrids, a general RL load dynamic model is considered in this paper. The state equations of the RL load connected at i^{th} node are

$$\frac{di_{loadDi}}{dt} = \frac{-R_{loadi}}{L_{loadi}} i_{loadDi} + \omega i_{loadQi} + \frac{1}{L_{loadi}} v_{bDi} \quad (59)$$

$$\frac{di_{loadQi}}{dt} = \frac{-R_{loadi}}{L_{loadi}} i_{loadQi} - \omega i_{loadDi} + \frac{1}{L_{loadi}} v_{bQi} \quad (60)$$

Hence, for a network with *p* load points the small-signal state-space model of loads is given by (61).

$$\left[\ \Delta \dot{i}_{load}\ \right] = A_{LOAD} \left[\ \Delta i_{load}\ \right] + B_{1LOAD} \left[\Delta v_{bDQ}\right] + B_{2LOAD} \Delta\omega \quad (61)$$

In (61)

$$\left[\ \Delta i_{load}\ \right] = \left[\Delta i_{load\ 1}\ \Delta i_{load\ 2}\ ...\ \Delta i_{load\ p}\right]^T \quad (62)$$

$$A_{LOAD} = \begin{bmatrix} A_{LOAD\ 1} & 0 & ... & 0 \\ 0 & A_{LOAD\ 2} & ... & 0 \\ ... & ... & ... & ... \\ 0 & 0 & ... & A_{LOAD\ p} \end{bmatrix}_{2p\times 2p} \quad (63)$$

$$B_{1LOAD} = \left[\ B_{1LOAD\ 1}\ B_{1LOAD\ 2}\ ...\ B_{1LOAD\ p}\ \right]^T$$
$$B_{2LOAD} = \left[\ B_{2LOAD\ 1}\ B_{2LOAD\ 2}\ ...\ B_{2LOAD\ p}\ \right]^T \quad (64)$$

where,

$$A_{LOADi} = \begin{bmatrix} \frac{-R_{loadi}}{L_{loadi}} & \omega_0 \\ -\omega_0 & \frac{-R_{loadi}}{L_{loadi}} \end{bmatrix} B_{2LOADi} = \begin{bmatrix} I_{loadQi} \\ -I_{loadDi} \end{bmatrix}$$
$$B_{1LOADi} = \begin{bmatrix} ... & \frac{1}{L_{loadi}} & 0 & ... \\ ... & 0 & \frac{1}{L_{loadi}} & ... \end{bmatrix}_{2\times(2m)} \quad (65)$$

D. Complete microgrid model

It can be seen in (42), (52) and (61) that the node voltages are treated as inputs to each sub-system. To establish the node voltage a virtual resistor r_N is assumed at each node of the network. The resistance of virtual resistor is chosen sufficiently large such that its introduction would have minimum influence on the dynamic stability of the system. Hence, the voltage of i^{th} node is given by

$$v_{bDi} = r_N \left(i_{oDi} - i_{loadDi} + i_{lineD\ i,j}\right) \quad (66)$$

$$v_{bQi} = r_N \left(i_{oQi} - i_{loadQi} + i_{lineQ\ i,j}\right) \quad (67)$$

In symbolic form, for a network with *m* nodes

$$\left[\ \Delta v_{bDQ}\ \right] = R_N(M_{INV}\left[\Delta i_{oDQ}\right] + + M_{LOAD}\left[\Delta i_{load}\right] + M_{NET}\left[\Delta i_{line}\right]) \quad (68)$$

In (68), matrix R_N is of size $2m \times 2m$, whose diagonal elements are equal to r_N. The mapping matrix M_{INV} is of size $2m \times 2s$, which maps the inverter connection points onto network nodes. For example, if i^{th} inverter is connected at j^{th} node, the element $M_{INV}(j,i)$ will be 1 and all the other elements in that row will be 0. Similarly, M_{LOAD} is of size $2m \times 2p$ maps load connection points onto the network nodes with -1. Matrix M_{NET} of size $2m \times 2n$ maps the connecting lines onto the network nodes. Here care should be taken to put either +1 or -1 based on whether the given line current is leaving or entering the node.

Now, the complete microgrid small-signal state-space model and hence the system state matrix (as given in equation (69)) can be obtained by using the individual sub-system models given by (42), (43), (52), (61) and (68).

$$\begin{bmatrix} \Delta \dot{x}_{inv} \\ \Delta i_{line} \\ \Delta i_{load} \end{bmatrix} = A_{mg} \begin{bmatrix} \Delta x_{inv} \\ \Delta i_{line} \\ \Delta i_{load} \end{bmatrix} \quad (69)$$

The complete system state matrix A_{mg} is given in (70). The small-signal flow among all the sub-modules is shown in Fig. 2.

III. EIGENVALUE AND SENSITIVITY ANALYSIS

The eigenvalue concept of control theory has been extensively used to determine the stability of conventional power systems. Eigenvalues, termed *modes*, are the solution of characteristic equation of a system's linearized state matrix [14]. Eigenvalues reveal the different frequency components in the system and their available damping.

A. Sensitivity analysis

Further information on the origin of different frequency components can be obtained by observing the participation of different state variables in a particular mode [14]. This can be achieved with a sensitivity analysis conducted on the system state matrix. The sensitivity factor p_{ki}, given by (71), is the measure of the association between the state variables and the modes and is equal to the sensitivity of the eigenvalue λ_i to the diagonal element a_{kk} of the system state matrix. Sensitivity factors can be calculated using left and right eigenvectors.

$$p_{ki} = \frac{\partial \lambda_i}{\partial a_{kk}} \quad (71)$$

IV. EXPERIMENTAL VERIFICATION OF MODEL

A 220 V (per phase RMS), 50 Hz prototype microgrid was built to test and verify the model results. As shown in Fig. 10 the test system consist of three inverters of equal rating with two load banks, one at each bus 1 and bus 3. These inverters are controlled to share the real and reactive powers over the lines 1 and 2. System parameters are given in Table I. It can be seen that the prototype system represents a general possible case of a microgrid. Network is more resistive as is the case in low voltage distribution systems. DG1 and DG2 are located relatively close together compared to DG3. In this test system only resistive loads were used to verify the model. A resistive

$$A_{mg} = \begin{bmatrix} A_{INV} + B_{INV}R_N M_{INV} C_{INVc} & B_{INV}R_N M_{NET} & B_{INV}R_N M_{LOAD} \\ B_{1NET}R_N M_{INV} C_{INVc} + B_{2NET} C_{INV\omega} & A_{NET} + B_{1NET}R_N M_{NET} & B_{1NET}R_N M_{LOAD} \\ B_{1LOAD}R_N M_{INV} C_{INVc} + B_{2LOAD} C_{INV\omega} & B_{1LOAD}R_N M_{NET} & A_{LOAD} + B_{1LOAD}R_N M_{LOAD} \end{bmatrix} \quad (70)$$

load of 5.8 kW (=25 Ω per phase) at bus 1 and 7.3 kW (=20 Ω per phase) at bus 2 is considered as an initial operating point.

The droop gains of all the inverters were chosen to be equal so that they share equal fundamental power. The nominal frequency droop was 0.3% at the maximum real power output, whereas the nominal voltage droop was 2% at the maximum reactive power output. The voltage controller was designed to have a bandwidth of 400 Hz while the current controller was designed for 1.6 kHz bandwidth with good rejection of high-frequency disturbance. Although, the control was implemented in discrete-time domain, the equivalent continuous domain gains are provided (in Table. I) to construct the model.

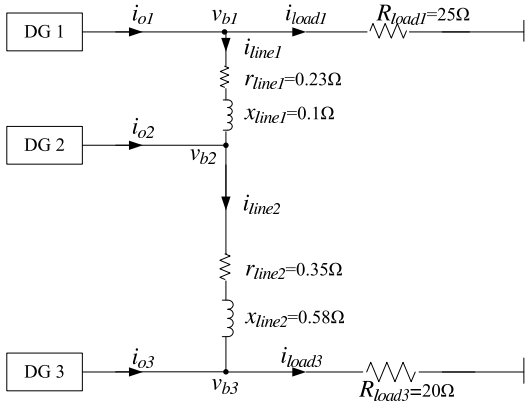

Fig. 10. Test system

TABLE I
TEST SYSTEM PARAMETERS

Inverter parameters (10 kVA rating)			
Parameter	Value	Parameter	Value
f_s	8 kHz	m_p	9.4e-5
L_f	1.35 mH	n_q	1.3e-3
C_f	50 μF	K_{pv}	0.05
r_f	0.1 Ω	K_{iv}	390
L_c	0.35 mH	K_{pc}	10.5
r_{Lc}	0.03Ω	K_{ic}	16e3
rating	10 kVA	F	0.75
Network and Load parameters (see Fig. 10)			

A. Modeling Results

A complete model of the test system was obtained using the procedure outlined in section II. Initial conditions of the system are given in Table II. These steady-state operating point conditions were obtained from MATLAB/SIMULINK time-step simulation of the system. However, it is possible to use a more general load-flow solution as is often done in conventional power system modeling to obtain initial steady-state conditions [14].

Fig. 11 shows the complete eigenvalues of the system for the initial conditions given in Table II. It can be seen that a large range of frequency components exist and that these fall in to three different clusters. Using (71), participation of different states in these eigenvalues was obtained. It can be seen that the high frequency modes in cluster '3' are sensitive to the state variables of LCL filter block of inverters and line currents. The modes in cluster '2' are largely sensitive to the state variables of voltage controller, current controller, and output LC filter. The low frequency dominant modes shown in cluster '1' are largely sensitive to the state variables of power controller.

TABLE II
INITIAL CONDITIONS

Par.	Value	Par.	Value
V_{od}	[380.8 381.8 380.4]	V_{oq}	[0 0 0]
I_{od}	[11.4 11.4 11.4]	I_{oq}	[0.4 -1.45 1.25]
I_{ld}	[11.4 11.4 11.4]	I_{lq}	[-5.5 -7.3 -4.6]
V_{bd}	[379.5 380.5 379]	V_{bq}	[-6 -6 -5]
ω_0	[314]	δ_0	[0 1.9e-3 -0.0113]
I_{line1d}	[-3.8]	I_{line1q}	[0.4]
I_{line2d}	[7.6]	I_{line2q}	[-1.3]

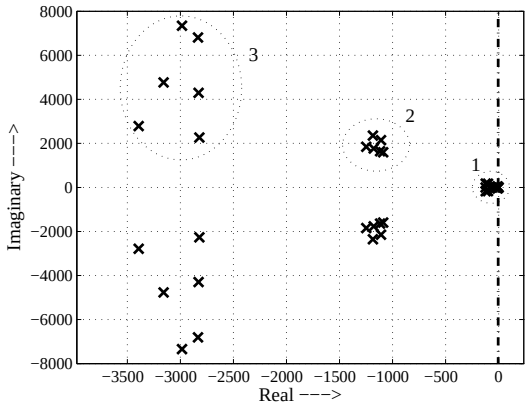

Fig. 11. The eigenvalue spectrum of the system indicating various modes

Fig. 12 shows the trajectory of the two-pairs of complex-conjugate dominant low frequency eigenvalues (part of cluster 1) as a function of real power droop gain m_p of all the three inverters. The eigenvalues marked with λ_{1-2} are largely sensitive to the state variables of real power part of the power controllers of inverters 1 and 2, as given in Table III. Similarly, eigenvalue marked as λ_{1-3} are highly sensitive to the state variables of real power part of the power controllers of inverters 1 and 3. It is therefore apparent that the modes λ_{1-2} and λ_{1-3} represent the dynamics of real power sharing

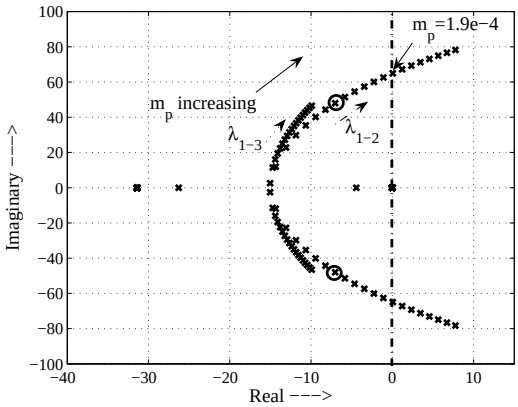

Fig. 12. Trace of low-frequency modes: $1.57e^{-5} \leq m_p \leq 3.14e^{-4}$

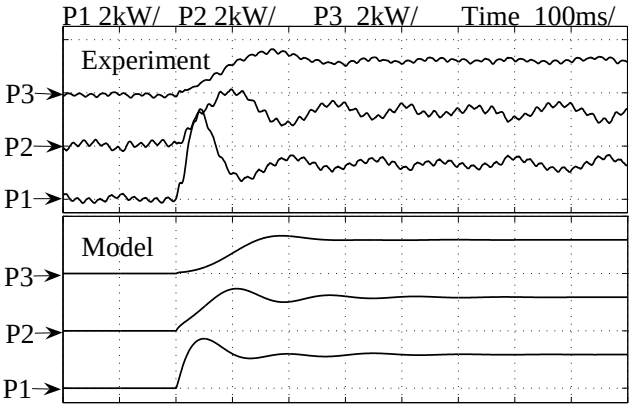

Fig. 13. Output power (filtered) response of micro-sources with 3.8 kW of step change in load power at bus 1

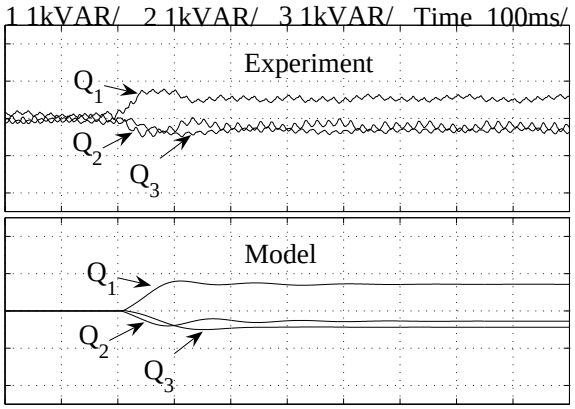

Fig. 14. Reactive power exchange between the micro sources with 3.8 kW of step change in load power at bus 1

of the DGs. However, these modes are also sensitive to the reactive power. This in fact represents the coupling of real and reactive powers in the network due the presence highly resistive lines.

Fig. 12 shows that as m_p is increased, modes λ_{1-2} and λ_{1-3} move towards unstable region making the system more oscillatory and eventually leading to instability. It is to be noted that large droop gain is necessary to improve the transient response of DGs, whereas a low-pass filter with low cut-off frequency is needed to achieve good attenuation of high frequency distortion components in the measured power and to avoid any interaction with inner current controllers. Also, from table III it can be observed that the most dominant mode λ_{1-2} is highly sensitive to the states of the power controller of inverter 2. Hence, in this system, inverter 2 is the most critical element from the point of view of system stability.

TABLE III
SENSITIVITY OF LOW FREQUENCY DOMINANT MODES

Sensitivity of λ_{1-2}		Sensitivity of λ_{1-3}	
state	participation	state	participation
P_1	0.15	P_1	0.12
Q_1	0.05	Q_1	0.06
P_2	0.3	P_3	0.32
Q_2	0.03	Q_3	0.03
δ_2	0.5	δ_3	0.57
remaining states $\leq$0.005			

B. Experimental results

In this section results obtained from the model are verified against the experimental testing using the system described at the beginning of Section IV. First, to verify the low frequency modes within the model, a disturbance in load current $i_{load\ 1}$ was modeled. This requires the addition of a controlled current source in parallel to R_{load1} shown in Fig.10 and the addition of a disturbance term to (69). The disturbance was chosen to be equal to the step change of 3.8 kW real power. Then, the experimental system was excited with the same 3.8 kW step change in load at bus 1. A second of tests was used to examine the high frequency modes. Due to the presence of significant damping, a large disturbance in the load was needed to capture the high frequency modes. A step change of 27 kW (from no load) at bus 1 was considered.

Figures 13, 14, 15 and 16 shows the response of state variables P, Q, v_{od} and i_{ld} of all the three inverters obtained from the model and experiment. It is to be noted that the waveforms corresponding to the experimental results are actually the internal variables of inverters that were captured by using on-board D/A converters. Also, all these figures depict only the variation in the signal from their initial point (relative change).

Fig. 13 shows the DG fundamental output power response for a 3.8 kW step change in load 1, for both the model and experimental system. The dominant, poorly damped low frequency modes λ_{1-2} (marked with a circle in Fig. 12) of frequency 7.2 Hz can be clearly observed in the fundamental power. Although, a slight difference in the magnitude exists, the response obtained from the model matches with the response obtained from the practical test system. Due to a slight unequal dc off-set in the measured output phase currents a small 50 Hz component was observed in the output power in the experimental case.

In Fig. 13 it can be seen that DG1 which is near to the changed load took the major part of the transient, whereas

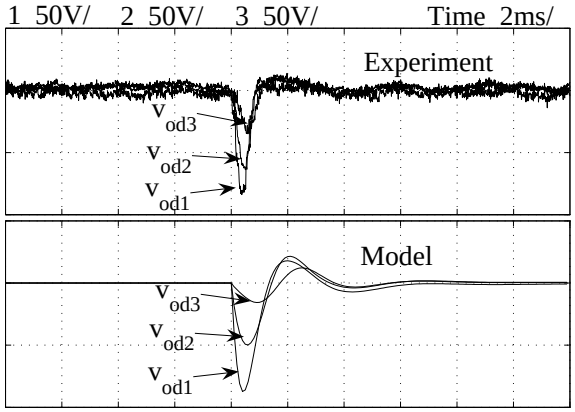

Fig. 15. Output voltage response with 27 kW of step change in load power at bus 1

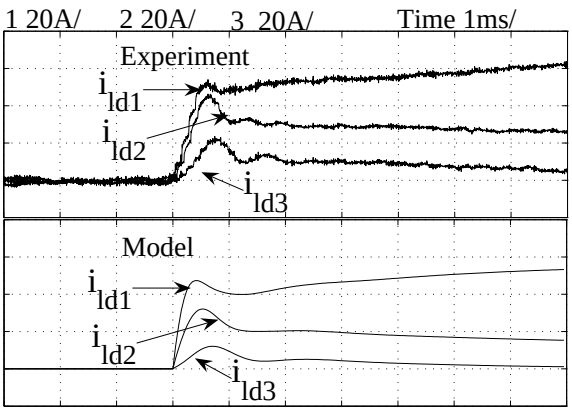

Fig. 16. Inductor current response

DG2 and DG3 have responded slower, depending on the effective impedance seen from the load point. Hence, during large changes in the load, closely located DGs may be overloaded and can be tripped out due to the limited overload capacity of the inverters.

Fig. 14 shows the fundamental reactive power sharing. It can be seen that a considerable amount of reactive power was exchanged between the inverters due to the presence of large resistance in the lines. This can be reduced by increasing the voltage magnitude droop but will be at the expense of voltage quality. This is one of the major limitations of conventional droop control applied in low voltage grids [15][16]. Again, it can be observed that the experimental results closely match with the model results.

Fig. 15 depicts the output voltage response of all the three inverters for a 27 kW load change. The high frequency modes of frequency around 350 Hz in cluster '2' shown in fig. 11 can be observed in the output voltage response. Although, a slight difference exists in the magnitude of response obtained from the linear model compared ro the test system, the oscillatory response in both cases matches. Also, the response obtained from the experimental set-up is more damped that of the model. It is to be noted that the participation of the output voltage state variable is the maximum in these modes. It would be interesting to investigate the possible excitation of these modes under harmonic loads because, the lower order significant harmonic frequencies will fall in the range of frequencies of these modes. However, this is not in the scope of this paper.

Fig. 16 shows the inductor current response of all the three inverters. In this case, high frequency modes with a frequency of around 800 Hz in cluster '3' in Fig. 11 can be observed in the response. It was observed that these modes are highly sensitive to the load condition of the system and that this determines their damping.

V. CONCLUSIONS

In this paper a small-signal state-space model of a microgrid is presented. The model includes inverter low frequency dynamics, high frequency dynamics, network dynamics and load dynamics. All the sub-modules are individually modeled and are then interfaced on a common reference frame to obtain the complete model of the microgrid.

The results of the model were analysed in terms of the system eigenvalues and their sensitivity to different states. With the help of this analysis the relation between different modes and system parameters was established. It was observed that the dominant low-frequency modes are highly sensitive to the network configuration and the parameters of the power sharing controller dynamics of the micro sources. The high frequency modes are largely sensitive to the inverter high frequency controller dynamics, network dynamics and load dynamics.

Results obtained from the model were verified experimentally on a prototype microgrid. It was observed that the model successfully predicts the complete microgrid dynamics both in low as well as in high frequency range.

Small signal modeling has had a long history of use in conventional power system. The inverter models (and the inclusion of network dynamics) illustrated here allow microgrids to be designed to achieve stability margin required of reliable power systems.

VI. ACKNOWLEDGMENT

This work was supported by the microgrids workpackage of the Supergen Future Network Technologies Consortium (www.supergen-networks.org.uk). Supergen is funded by several research counsels and led by EPSRC.

REFERENCES

[1] R. H. Lasseter, "Microgrids," *Power Engineering Society Winter Meeting*, vol. 1, pp. 305–308, Jan. 2002.

[2] A. Arulampalam, M. Barnes, A. Engler, A. Goodwin, and N. Jenkins, "Control of power electronic interfaces in distributed generation microgrids," *International Journal of Electronics*.

[3] "Integration of distributed energy resources: The certs microgrid concept," *CERT report*.

[4] M. S. Illindala, P. Piagi, H. Zhang, G. Venkataramanan, and R. H. Lasseter, "Hardware development of a laboratory-scale microgrid phase 2: Operation and control of a two-inverter microgrid," *National Renewable Energy Report*, March 2004.

[5] E. A. A. Coelho, P. Cortizo, and P. F. D. Gracia, "Small signal stability for parallel-connected inverters in stand-alone ac supply systems," *IEEE Transactions on Industrial Applications*, vol. 38, no. 2, pp. 533–542, March/April 2002.

[6] J. M. Guerrero, L. G. V. na, M. Castilla, and J. Miret, "A wireless controller to enhance dynamic performance of parallel inverters in distributed generation systems," *IEEE Transactions on Power Electronics*, vol. 19, no. 5, pp. 1205–1213, Sept. 2004.
[7] A. L. Dimeas and N. D. Hatziargyriou, "Operation of a multiagent system for microgrid control," *IEEE Transactions on Power Systems*, vol. 20, no. 3, pp. 1447–1455, Aug. 2005.
[8] M. Prodonovic, T. Green, and H. Mansir, "A survey of control methods for parallel three-phase inverters connection," *IEE PEVD Conference Publication*, no. 475, pp. 472–477, Sep. 2000.
[9] M. C. Chandorker, D. M. Divan, and A. Rambabu, "Control of parallel connected inverters in stand-alone ac supply systems," *IEEE Transactions on Industrial Applications*, vol. 29, no. 1, pp. 136–143, Jan./Feb. 1993.
[10] J. M. Undrill, "Dynamic stability calculations for an arbitrary number of interconnected synchronous machines," *IEEE Transactions on Power Apparatus and Systems*, vol. PAS-87, no. 3, pp. 835–845, March 1968.
[11] M. N. Marwali, J. Jung, and A. Keyhani, "Control of distributed generation systems - part ii: Load sharing control," *IEEE Transactions on Power Electronics*, vol. 19, no. 6, pp. 1551–1561, Nov. 2004.
[12] M. Prodanovic, "Power quality and control aspects of parallel connected inverters in distributed generation," Ph.D. dissertation, Imperial College, University of London, 2004.
[13] M. N. Marwali and A. Keyhani, "Control of distributed generation systems - part i: Voltages and current control," *IEEE Transactions on Power Electronics*, vol. 19, no. 6, pp. 1541–1550, Nov. 2004.
[14] P. Kundur, *Power system stability and control*. McGraw Hill, USA, 1994.
[15] A. Tuladhar, H. Jin, T. Unger, and K. Mauch, "Control of parallel inverters in distributed ac power systems with consideration of line impedance effect," *IEEE Transactions on Industrial Applications*, vol. 36, no. 1, pp. 131–138, Jan./Feb. 2000.
[16] A. Engler, "Applicability of droops in low voltage grids," *International journal of distributed resources*, vol. 1, no. 1, pp. 3–15, Sept. 2004.

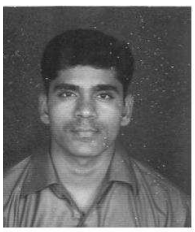

Nagaraju Pogaku (S'04) received the B. Engg. degree in electrical & electronics engineering from Osmania University, Hyderabad, India in 2000 and M. Tech. degree in electrical engineering (with a specialization in power electronics and power systems) from Indian Institute of Technology Bombay, India in 2003. He is currently a Ph.D. student in the Department of Electrical & Electronics Engg., Imperial College London, U. K. His research interests include distributed generation, microgrid, application of power electronics to power systems and power system deregulation.

Milan Prodanović (M '01) received a B.Sc. degree in electrical engineering from the University of Belgrade, Serbia in 1996 and obtained the Ph.D. degree in Imperial College, London, UK in 2004. He is currently a research associate at Imperial College. From 1997 to 1999 he was engaged with GVS engineering company, Serbia, developing power electronic circuits and control algorithms for inverter and UPS systems. His research interests are in digital control of power electronic systems, computer-aided analysis and design of power converters, power quality, micro-grids and distributed generation.

Tim C Green (M '89, SM '02) received a B.Sc. (Eng) (first class honours) from Imperial College, London, UK in 1986 and a Ph.D. from Heriot-Watt University, Edinburgh, UK in 1990. Both degrees were in electrical engineering. He was a Lecturer at Heriot Watt University until 1994 and is now a Professor of Electrical Power Engineering at Imperial College London and Deputy Head of the Control and Power Research Group. His research interest is in using power electronics and control to enhance power quality and power delivery. This covers interfaces and controllers for distributed generation, micro-grids, active distribution networks, FACTS and active power filters. He has an additional line of research in power MEMS and energy scavenging. He is a Chartered Engineer in the UK and MIEE.